ACS APPLIED MATERIALS & INTERFACES

Research Article

www.acsami.org

Pore Development in Carbonized Hemoglobin by Concurrently Generated MgO Template for Activity Enhancement as Fuel Cell Cathode Catalyst

Jun Maruyama,*[,†] Takahiro Hasegawa,[†] Taiji Amano,[‡] Yasuji Muramatsu,[‡] Eric M. Gullikson,[§] Yuki Orikasa,[⊥] and Yoshiharu Uchimoto[⊥]

[†]Environmental Technology Research Division, Osaka Municipal Technical Research Institute, 1-6-50, Morinomiya, Joto-ku, Osaka 536-8553, Japan,

[‡]Department of Material Science and Chemistry, Graduate School of Engineering, University of Hyogo, 2167 Shosha, Himeji, Hyogo 671-2201, Japan,

[§]Center for X-ray Optics, Lawrence Berkeley National Laboratory, 1-Cyclotron Road, Berkeley, California 94720, United States ,

[⊥]Department of Interdisciplinary Environment, Graduate School of Human and Environmental Studies, Kyoto University, Yoshida-nihonmatsu-cho, Sakyo-ku, Kyoto 606-8501, Japan

Supporting Information

ABSTRACT: Various carbon materials with a characteristic morphology and pore structure have been produced using template methods in which a carbon-template composite is once formed and the characteristic features derived from the template are generated after the template removal. In this study, hemoglobin, which is a natural compound that could be abundantly and inexpensively obtained, was used as the carbon material source to produce a carbonaceous noble-metal-free fuel cell cathode catalyst. Magnesium oxide was used as the template concurrently generated with the hemoglobin carbonization from magnesium acetate mixed with hemoglobin as the starting material mixture to enable pore development for improving the activity of the carbonized hemoglobin for the cathodic oxygen reduction. After removal of the MgO template, the substantially developed pores were generated in the carbonized hemoglobin with an amorphous structure observed by total-electron-yield X-ray absorption. The extended X-ray absorption fine structure at the Fe-*K* edge indicated that Fe was coordinated with four nitrogen atoms ($Fe-N_4$ moiety) in the carbonized hemoglobin. The oxygen reduction activity of the carbonized hemoglobin evaluated using rotating disk electrodes was dependent on the pore structure. The highly developed pores led to an improved activity.

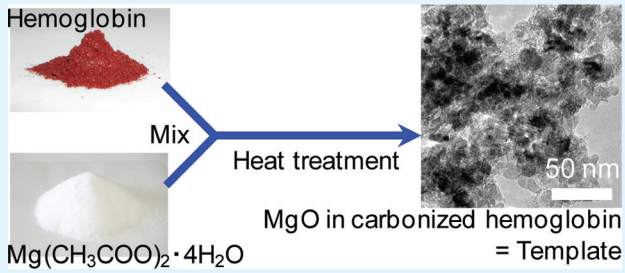

KEYWORDS: *hemoglobin, carbonization, template, magnesium oxide, fuel cell, electrode catalyst, oxygen reduction*

INTRODUCTION

Carbon materials are able to have a characteristic morphology and pore structure when the carbon precursors are heat-treated with templates, which maintain their morphology during the heat treatment to generate the carbon-template composite. The templates are then removed to leave the carbon materials reflecting the morphology of the templates. Many materials have been applied to the templates, such as clays with layered structures,[1] porous almina,[2] zeolites,[3] mesoporous silica,[4,5] and silica nanoparticles.[6,7] One of the main disadvantages of this template method is the need to dissolve and remove the templates under harsh conditions often using hydrofluoric acid or strong base solutions.

Recently, Morishita et al. reported a new template method using magnesium oxide nanoparticles, in which thermoplastic polymers were mixed with Mg acetate or Mg citrate.[8] The nanosized and well-dispersed MgO particles were concurrently generated with the carbonization, and highly developed pores were left behind after the MgO removal. The significant advantages of this method are ease of preparation of the carbon-template composite; the mixing the starting materials is possible in solutions and also in powders, and facility of the removal of the MgO, which is possible even with weak acid solutions like acetic acid. Quite recently, we found that this MgO template method could be applied to a small organic molecule and an iron salt as the starting materials to form a carbon material with developed pores and catalytic activity for the cathodic oxygen reduction.[9]

Our previous studies have shown that the carbon materials formed from heme-containing proteins, such as catalase and

Received: September 28, 2011
Accepted: November 17, 2011
Published: November 17, 2011

hemoglobin, function as a catalyst in the cathode of a polymer electrolyte fuel cell (PEFC).[10−14] The PEFC is a clean and efficient new energy system[15] and expected to improve the global environment by its widespread use after realization of the active and stable noble-metal-free catalysts free from cost inflation and resource limitations.[16] Hemoglobin is one of the materials meeting these requirements based on its abundance and inexpensiveness because hemoglobin could be abundantly obtained (about 2 million tons per year), especially from the meat industry that produces more than 200 million tons of meat per year around the world and discards hemoglobin-containing blood as waste. Although the activity and durability were insufficient to replace conventional Pt-based catalysts, the effectiveness of the development of pores inside the carbon material on the activity enhancement were shown in a previous study.[13]

In this study, we attempted to further develop the pores in the carbonized hemoglobin by applying the MgO template method for the activity enhancement. Magnesium acetate, $Mg(CH_3COO)_2$, was used as the template precursor, added to a hemoglobin solution, and completely mixed. The $Mg(CH_3COO)_2$ concentration was less than that causing the salting-out phenomenon. The two-step carbonization procedure was used to produce active catalysts.[12,13] The temperature of the first step was 400 °C for the secure formation of MgO[8] and Fe with the 2+ oxidation state in the carbonized hemoglobin,[12,13] which is required as an O_2 bonding site during the first step of the multistep O_2 reduction reaction.[17] We found that the pores were highly developed inside the carbonized hemoglobin and that the activity for the O_2 reduction was enhanced when compared to those produced in the previous studies.

EXPERIMENTAL SECTION

Materials. Hemoglobin from bovine blood and magnesium acetate tetrahydrate, $Mg(CH_3COO)_2{\cdot}4H_2O$, were purchased from Sigma and Wako Pure Chemical Industries, respectively, and used as received. A commercially available catalyst of 50 wt % platinum on Vulcan XC-72R carbon (Pt/C, Johnson Matthey) was used as the conventional Pt-based catalyst. High-purity water was obtained by circulating ion-exchanged water through an Easypure water-purification system (Barnstead, D7403). Perchloric acid (70%, Tama Chemical, analytical grade) was diluted with high-purity water to prepare 0.1 mol dm^{-3} $HClO_4$ as the electrolyte for the O_2 reduction measurements. Solutions of Nafion as the perfluorosulfonate ion-exchange resin [equivalent weight (molar mass/mol of ion-exchange site) = 1100, 5, and 20 wt % dissolved in a mixture of lower aliphatic alcohols and 15−20% water] were purchased from Aldrich. In order to prepare dispersions of the catalyst, the Nafion solutions, high purity water, and 2-propanol (Kanto Chemical) were used. Nafion 112 was used as the electrolyte membrane for the fuel cell test. The membrane was successively immersed in 3% H_2O_2, high-purity water, 1 mol dm^{-3} H_2SO_4, and high-purity water at boiling temperatures, and stored in high-purity water before use.

Formation of Catalyst. Hemoglobin was dissolved in high-purity water to prepare a 5 wt % aqueous solution. An aqueous $Mg(CH_3COO)_2$ solution was prepared by dissolving $Mg(CH_3COO)_2{\cdot}4H_2O$ in the same amount of water as the hemoglobin solution. These two solutions were mixed and stirred for 1 h. The weight ratio of $Mg(CH_3COO)_2$/hemoglobin in the mixture, *m*, was 1, 2, 3, 4, or 5. The solution of the hemoglobin−$Mg(CH_3COO)_2$ mixture was frozen and placed in a vacuum chamber overnight. The mixture was then heated at 50 °C under vacuum to completely dry it. The dried mixture was heated in flowing Ar at 400 °C for 10 h after raising the temperature at 5 °C min^{-1} and then finely ground to obtain the catalyst precursor. The precursor formed from the hemoglobin−$Mg(CH_3COO)_2$ mixture with the ratio *m* was labeled CHbMg*m*s400 (*m* = 1, 2, 3, 4, or 5). The precursor was heated in flowing Ar at 900 °C for 2 h after raising the temperature at 5 °C min^{-1}. The sample was finely ground again and a treatment with an acid solution was carried out to remove any soluble Mg and Fe species. The acid treatment was performed in boiling 2.5 mol dm^{-3} H_2SO_4 for 1 h, followed by filtering, washing with high-purity water, and drying in a vacuum at room temperature. The carbonaceous material formed from CHbMg*m*s400 was labeled CHbMg*m*s400900.

Characterization of Catalyst. The Fe content in the catalyst was measured by inductively coupled plasma atomic emission spectrophotometry (ICP-AES) using an ICPS-8100 system (Shimadzu) after the combustion of the carbon matrix and the dissolution of the residue by boiling 0.5 mol dm^{-3} H_2SO_4. The adsorption isotherm of N_2 onto the catalyst was measured using an automatic N_2 adsorption apparatus (BelsorpII, Nihon Bell) at −196 °C. The specific surface area was determined from the Brunauer−Emmet−Teller (BET) plot of the isotherm. The differential pore-volume distributions were also determined by the Dollimore-Heal method using the isotherm. The X-ray diffraction (XRD) was performed using an automated RINT 2500 X-ray diffractometer (Rigaku) with Cu Kα radiation. The data acquisition was carried out in the $\theta/2\theta$ step scanning mode at a speed of 1° min^{-1} with a step size of 0.02° (2θ). A transmission electron micrograph (TEM) was obtained using a JEM-2100IM (JEOL). The X-ray absorption spectra (XAS) in the C-*K* region and Fe-*L* region were measured using synchrotron radiation (SR) at the beamline of BL-6.3.2[18] of the Advanced Light Source (ALS), Lawrence Berkeley National Laboratory. The energy resolutions ($E/\Delta E$) of the XAS measurements were 5000 for the C-*K* region and 1500 for the Fe-*L* region using a 1200 lines/mm grating and a 40 μm slit. All powder samples were placed on an indium sheet of the sample holder in the vacuum measurement chamber. The sample photocurrent induced by SR irradiation was them monitored during the SR photon energy scanning, which provided the total-electron-yield (TEY) XAS.[19,20] The TEY-XAS of the high-abrasion-furnace carbon black categorized as N330 in the American Standard Testing Material (ASTM) code and commercially available highly oriented pyrolytic graphite (HOPG) were measured as well as the carbon material formed in this study. The measurements of the extended X-ray absorption fine structures (EXAFS) at the Fe-*K* edge of the catalysts were performed in the transmission mode in air at room temperature using SR at the beamlines of BL14B2 and BL01B1 of the SPring8 in the Japan Synchrotron Radiation Research Institute. Fourier transformation was performed on the k^3-weighted EXAFS spectra using the REX2000 program (Rigaku) to calculate the pseudoradial distribution functions (RDFs). The coordination number, the distance between the absorbing atom and the nearest scattering atoms, and the Debye−Waller factor were calculated. The phase shift and the back scattering factor were calculated using FEFF8.2.

Evaluation of Catalytic Activity Using Rotating Disk Electrodes. The activity of the catalyst was evaluated by fixing it on the surface of a rotating glassy carbon disk electrode (GC RDE) as a catalyst layer and immersing it in 0.1 mol dm^{-3} $HClO_4$.[21−23] An aliquot of 10 mg of the finely ground catalyst and 10 mg of carbon black (Vulcan XC-72R, Cabot) as the electron-conductive agent were added to 1 cm^3 of the 5 wt % Nafion solution. The addition of carbon black was necessary to improve the electron conduction inside the catalyst layer.[21] The mixture was ultrasonically dispersed to produce a catalyst paste. A GC RDE (Hokuto Denko), which consisted of a GC rod sealed in a Kel-F holder, was polished with 2000 grit emery paper (Sumitomo 3M) and then ultrasonically cleaned in high-purity water for use as a support for the catalyst layer. The geometric surface area of the electrode was 0.196 cm^2 (diameter, 5 mm). A 6 mm^3 volume of the paste was pipetted onto the GC surface, and to shield it from the irregular air stream generated by a ventilator, the electrode was immediately placed under a glass cover until the layer was formed. After removal of the glass cover, the layer was further dried overnight at room temperature.

An electrochemical measurement system (HZ-5000, Hokuto Denko) and an RDE apparatus (HR-201, Hokuto Denko) equipped

with a glass cell were used for the cyclic voltammetry and the measurements of the current−potential relationships. The glass cell was cleaned by soaking it in a 1:1 mixture of concentrated HNO_3 and H_2SO_4, followed by a thorough rinsing with high-purity water and finally steam-cleaning.[24] The counter electrode was a Pt wire and the reference electrode was a reversible hydrogen electrode (RHE). All potentials were referred to the RHE. The current−potential relationships for the O_2 reduction were obtained in O_2-saturated 0.1 mol dm^{-3} $HClO_4$ at 25 °C at various rotation speeds. The scan rate of the potential was fixed at 10 mV s^{-1}. Prior to the measurement, the electrode was repeatedly and alternately polarized at 0.05 and 1.3 V.[25] The potential was finally stepped to 1.2 V and then swept in the negative direction to obtain the current−potential relationship. The background current was similarly measured in an Ar atmosphere without rotation.

Fuel Cell Tests. A catalyst layer was formed on 5 cm^2 carbon paper treated with polytetrafluoroethylene (ElectroChem) as the gas-diffusion layer. A catalyst paste for the cathode was prepared by ultrasonically dispersing 30 mg of the catalyst and 30 mg of carbon black in 1.2 cm^3 of a Nafion solution which was prepared by diluting a mixture of 0.286 cm^3 of the 20 wt % Nafion solution and 0.380 cm^3 of 2-propanol with high-purity water. A cathode was formed by spreading 1.0 cm^3 of the paste, followed by overnight drying. The amounts of the catalyst, carbon black, and Nafion were 5, 5, and 10 mg cm^{-2}, respectively. An anode was formed using a catalyst paste prepared by adding Pt/C to the mixture of the Nafion solution and high-purity water, then ultrasonically dispersing it. The paste was spread on the carbon paper and dried overnight at room temperature and 60 °C under a vacuum for 30 min. The amounts of Pt/C and Nafion were 1.0 mg cm^{-2} (Pt, 0.5 mg cm^{-2}) and 0.5 mg cm^{-2}, respectively. The electrodes and the electrolyte Nafion 112 membrane were pressed at 0.1 MPa and 150 °C for 10 min to form the membrane-electrode assembly, which was then incorporated into a single-cell apparatus (ElectroChem). The current−voltage relationship was measured at 80 °C under atmospheric pressure using a fuel cell station. Hydrogen and oxygen were supplied at 200 cm^3 min^{-1} and humidified at 80 °C. The current−voltage relationship was also measured by supplying air instead of oxygen at 1000 cm^3 min^{-1}. The current at 0.5 V was recorded during a continuous operation, in which hydrogen and air were supplied at 50 and 250 cm^3 min^{-1}, respectively.

RESULTS AND DISCUSSION

Formation of Carbon Materials and Pore Development. The decomposition of hemoglobin and Mg$(CH_3COO)_2$ caused a mass loss through the two heat-treatment steps to form the carbonaceous material and MgO. The mass loss was almost independent of *m* as shown in Figure 1a. Figure 2a shows the typical XRD spectra and the TEM images of the precursor formed by the first heat treatment at 400 °C (CHbMg3s400), the sample formed by the second heat treatment at 900 °C before the acid treatment, and the catalyst obtained after the acid treatment (CHbMg3s400900). The (111), (200), and (220) MgO diffraction peaks at 37, 43, and 62°, respectively, for the spectrum of the precursor indicated the MgO generation. The assignment of the small peaks at 15 and 26° is unknown at present. The TEM image of the precursor shows black particles attributed to MgO. The MgO particle growth by the second heat treatment is shown in both the XRD spectrum and the TEM images of the sample before the acid treatment. The MgO removal left amorphous carbon.

The carbon structure of the carbonaceous material was also investigated by the TEY-XAS measurements. Figure 3 shows the TEY-XAS in the C-*K* region of CHbMg3s400900 as well as carbon black (N330) and HOPG. A similar TEY-XAS was observed for the other *m*. It was recently found that the profile of the peak around 285 eV (the π^* peak) reflected the carbon structure.[19] The profile for CHbMg3s400900 was similar to

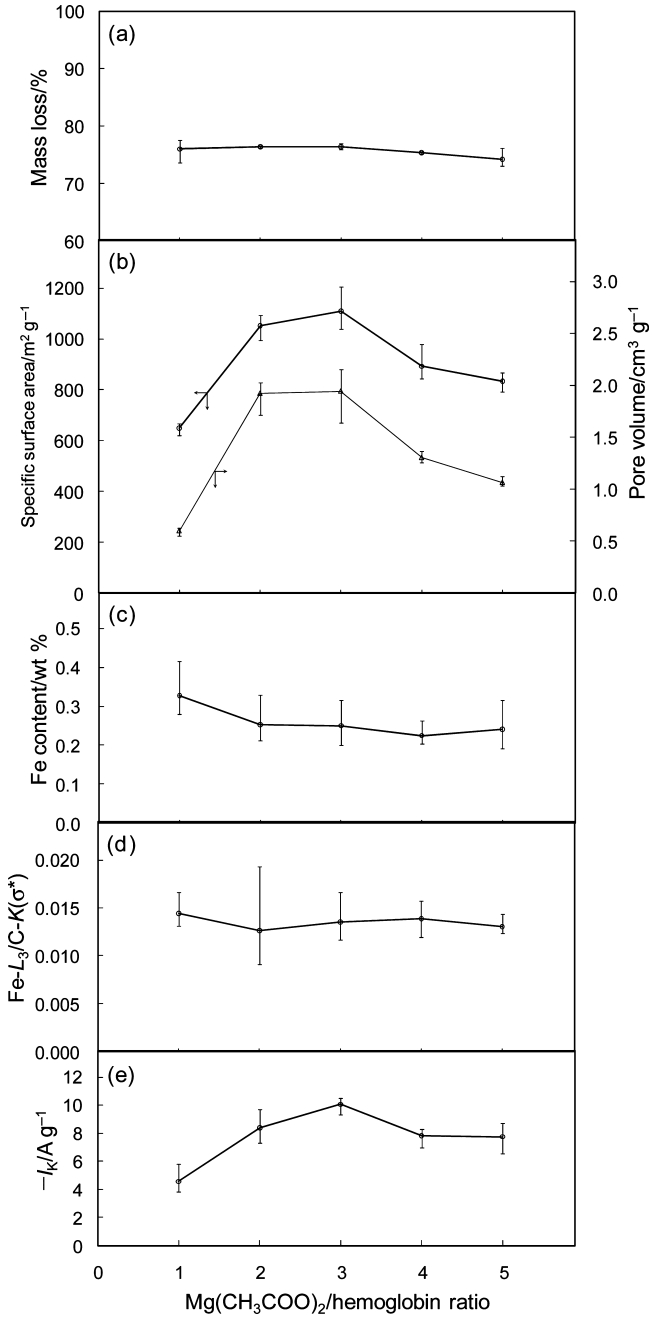

Figure 1. Dependence of characteristics of carbonized hemoglobin on the Mg$(CH_3COO)_2$/hemoglobin ratio in the dried starting material mixture: (a) mass loss, (b) specific surface area and pore volume, (c) Fe content, (d) TEY-XAS peak intensity ratio (Fe-L_3/C-$K(\sigma^*)$), (e) $-I_K$.

that of carbon black and different from that of HOPG. This result indicated that the carbon matrix structure was similar to that of carbon black, which is an amorphous, turbostratic structure consisting of randomly layered graphene sheets.

The typical differential pore-volume distributions of CHbMg*m*s400900 are shown in Figure 4. Those of the samples before the acid treatment were similar and that of *m* = 3 is shown in Figure 4. Before the acid treatment, the sample possessed very limited pores. The acid treatment caused the pore development. This result indicated that the pores in the carbonaceous material were the spaces that were occupied by MgO before the acid treatment.

dx.doi.org/10.1021/am2013294 | ACS Appl. Mater. Interfaces 2011, 3, 4837−4843

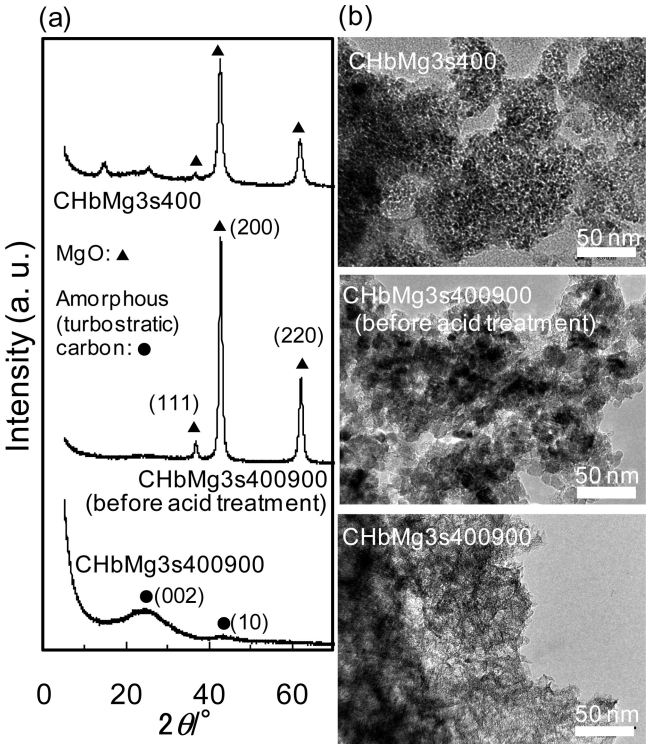

Figure 2. XRD spectra and TEM images of CHbMg3s400, CHbMg3s400900, and sample before acid treatment used to form CHbMg3s400900.

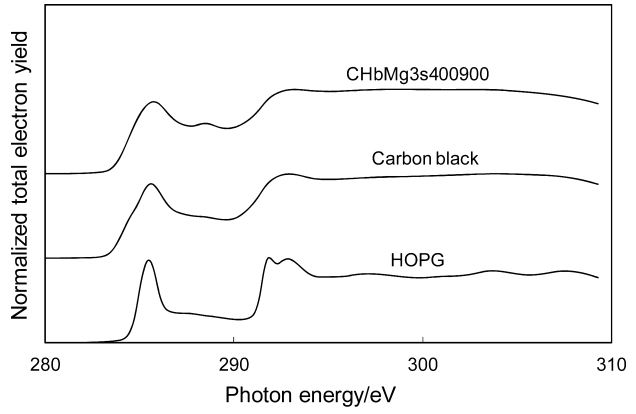

Figure 3. X-ray absorption spectra in the C-*K* region of CHbMg3s400900. Those of carbon black and HOPG are also shown as a reference of the carbon structure.

The extent of the pore development was dependent on *m*. Figure 1b shows the dependence of the specific surface area and the pore volume of the carbonaceous material on *m*. These two parameters of the pore structure increased with an increase in *m* up to *m* = 3 and then decreased. The maximum specific surface area and the pore volume were 1110 $m^2\ g^{-1}$ and 1.94 $cm^3\ g^{-1}$, respectively. These high values indicated the effectiveness of the MgO template method on the formation of carbon materials with substantially developed pores from hemoglobin.

State of Fe Inclusion in Carbon Material. The Fe content in the carbonaceous material was approximately independent of *m* (Figure 1c), except for the slightly high value at *m* = 1. The relative surface Fe concentration among the carbonaceous materials was evaluated by the peak intensity of the Fe-L_3 to that of C-*K* because the TEY-XAS provided

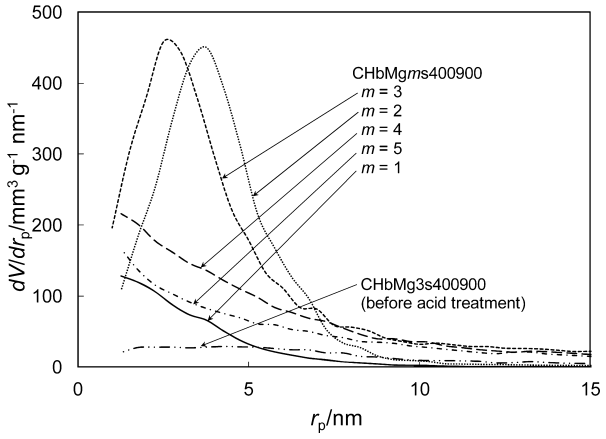

Figure 4. Differential pore-volume distributions of CHbMg*m*s400900 (*m* = 1−5) and the sample before the acid treatment used to form CHbMg3s400900. *V* is the pore volume and r_p is the pore radius.

information about the surface of the sample. The peak around 292 eV in the C-*K* region (the σ^* peak) was used as the reference because it was more appropriate for the quantitative analysis than the π^* peak based on our recent study.[20] The ratios of the peak intensities (Fe-L_3/C-$K(\sigma^*)$) were approximately independent of *m* (Figure 1d), in agreement with the Fe contents.

The EXAFS measurements at the Fe *K*-edge were performed in order to investigate the state of Fe in the carbonaceous materials. Figure 5 shows the Fe *K*-edge RDFs for

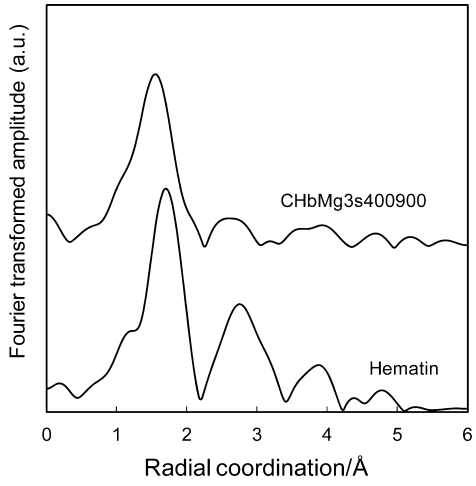

Figure 5. Pseudoradial distribution functions calculated by Fourier transformation of extended X-ray absorption fine spectra at the Fe *K*-edge for CHbMg3s400900 and hematin.

CHbMg3s400900, as well as hematin for comparison. Nearly the same RDFs were obtained, independent of *m*.

In the spectrum of hematin, the first peak at around 1.7 Å was attributed to four N atoms coordinating to the Fe(III) center. The shoulder at around 1.2 Å was attributed to OH^- coordinating perpendicular to the macrocyclic plane to the Fe center. The second peak at 2.7 Å was attributed to the C atoms, which were bound to the N atom in the pyrrolic ring and the bridging C connecting the pyrrolic rings.

The peaks similar to the first peaks for hematin were observed at 1.6 Å in the spectra of the carbonaceous material. Although it is recognized that the identification of the nearest

dx.doi.org/10.1021/am2013294 | ACS Appl. Mater. Interfaces 2011, 3, 4837–4843

neighbor atom only from the EXAFS result is difficult, it might be reasonable to assume the presence of the Fe−N_4 moiety in the carbonaceous material, which was derived from protoheme in hemoglobin. This assumption was based on our previous study showing the presence of the Fe−N_4 moiety in the carbonized catalase, which also contains protoheme,[10] and other previous studies reporting that the porphyrin-like structures were retained in the carbonaceous compounds after the pyrolysis of their precursor, which contained metal porphyrins, based on an analysis by X-ray photoelectron spectroscopy,[26] X-ray adsorption near-edge structure spectroscopy,[27] and Mössbauer spectroscopy.[28]

The curve fitting analysis was performed to calculate the coordination number of N to Fe (N) and the Fe−N distance (R_{Fe-N}) based on the assumption that the nearest neighboring atoms were N as described above, as well as the Debye−Waller factor (σ) representing the standard deviation from the average R_{Fe-N}.[29] The N for hematin and CHbMg3s400900 were both 4.0, supporting the presence of the Fe−N_4 moiety. The lower R_{Fe-N} in CHbMg3s400900 (1.99 Å) than in hematin (2.07 Å) indicated that the bond length between the Fe and the coordinating N was slightly shortened by the heat treatment. The σ in CHbMg3s400900 (0.095) was higher than that in hematin (0.071), but lower than that in CHb200900 (0.115) formed in our previous studies, in which CHb200900 was formed by the two-step heat treatment in Ar at 200 and 900 °C with 10% CO_2 in the second step for the pore development.[13] This σ decrease indicated an increase in the structural regularity of the Fe−N_4 moiety by the presence of MgO during the heat treatment, although the detailed mechanism of the increase is unclear at present.

Activity for Oxygen Reduction. The catalytic activity of the carbonaceous materials for the cathodic O_2 reduction was examined by measuring the oxygen reduction current at the catalyst layer in O_2-saturated 0.1 mol dm^{-3} $HClO_4$ at 25 °C using the GC RDEs. The O_2 reduction current at the catalyst layer without the influence of mass transfer in the solution, $-I_K$, was determined by[21]

$$-\frac{1}{I} = -\frac{1}{I_K} + \frac{1}{0.620nFAD^{2/3}c\nu^{-1/6}\omega^{1/2}}$$

where I is the reduction current measured using the RDE with the catalyst layer fixed on the surface after subtracting the background current, n is the number of electrons involved in the O_2 reduction per molecule, F is the Faraday constant, A is the geometric area of the GC electrode, D is the diffusion coefficient of O_2 in solution, c is the concentration of O_2 in solution, ν is the kinematic viscosity of the solution, and ω is the angular frequency of rotation. The sign of the cathodic current was taken as negative. The $-I_K$ values at 0.7 V vs RHE as an indicator of the activity of the catalyst layer are shown in Figure 1e. The $-I_K$ at 0.7 V was chosen based on the assumption that the kinetics could be largely reflected by the current at the potential without any experimental error caused by the low O_2 reduction current at the higher potential.

The $-I_K$ at 0.7 V increased with an increase in m up to 3 and then decreased. The main possible factors for the activity enhancement were the specific surface area and the pore volume of the carbonaceous material based on the comparison of the parameter dependences on m shown in Figure 1. The pore development led to the increase in the number of active sites through their exposure on the pore surface from the inside of the carbon matrix. The pore development also possessed the effect for enhancing the activity due to the increase in the availability of O_2 molecules for the individual active sites inside the pores in the catalyst. According to a theory proposed by Watanabe et al., there is a potential reaction space around each active site and the activity will decrease when overlapping of the space occurs by a decrease in the distance between the active site.[30] The increase in the specific surface area could avoid this interference between the active site, and the increase in the pore volume could expand the potential reaction space. We also fundamentally investigated the dependence of the activity for the O_2 reduction at the Pt-loaded activated carbon on the pore structure of the activated carbon support and found that the high specific surface area and pore volume were advantageous for the high activity.[31] The $-I_K$ at 0.7 V for CHbMg3s400900 exceeded the highest value among the catalysts that have already been formed from hemoglobin (8.75 A g^{-1} at CHb200900).

Fuel Cell Test. The PEFC was formed using CHbMg3s400900 that showed the highest $-I_K$ in the RDE measurements for the cathode and Pt/C for the anode. The relationships between the current density and the cell voltage and power density are shown in Figure 6. Compared to the best PEFC formed using the carbonized hemoglobin (CHb200900) in a previous study,[13] the current density above the cell voltage of 0.2 V and the maximum power density were higher in spite of the lower amount of the catalyst used in the cathode (5 mg cm^{-2}) than in the PEFC cathodes formed using the carbonized hemoglobin in the previous studies (10 mg cm^{-2}) (see Figure S1 in the Supporting Information). Although the performance was lower than that of the PEFC with the latest and highly active noble-metal-free cathode catalyst prepared using expensive and artificially synthesized raw materials,[32] the information obtained in this study could be useful in further enhancing the activity of the carbonized hemoglobin, which is derived from one of the abundant, renewable natural resources.

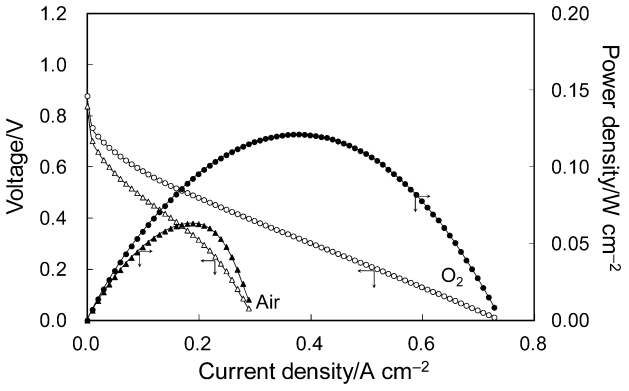

Figure 6. Relationships between current density and cell voltage (white symbols) and relationships between current density and power density (black symbols) for PEFC formed using 5 mg cm^{-2} of CHbMg3s400900 in the cathode and 1 mg cm^{-2} of Pt/C in the anode. The electrode area: 5 cm^2. Cell temperature: 80 °C. Gas humidification temperature: 80 °C. H_2 and O_2 were supplied at 200 cm^3 min^{-1} under atmospheric pressure (circle). H_2 and air were also supplied under atmospheric pressure at 200 and 1000 cm^3 min^{-1}, respectively (triangle).

In addition to the H_2/O_2 measurements, the PEFC performance and its degradation were also examined using H_2/air under atmospheric pressure due to its technological

dx.doi.org/10.1021/am2013294 | ACS Appl. Mater. Interfaces 2011, 3, 4837−4843

importance. Figure 6 also shows the relationships between the current density and the cell voltage and power density for the PEFC before degradation. The current density above the cell voltage of 0.2 V and the maximum power density were also higher than those for the PEFC formed using the carbonized hemoglobin in the previous studies. The current decrease during the continuous operation at 0.5 V is shown in Figure 7.

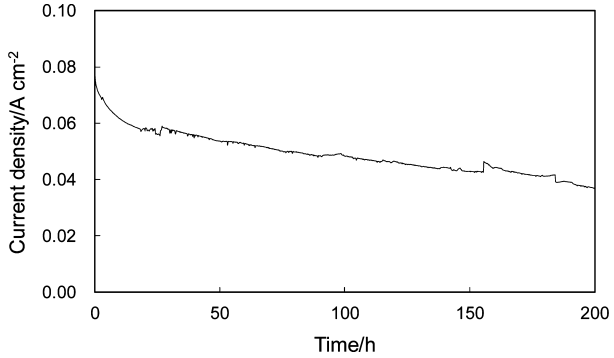

Figure 7. Change in current at 0.5 V during continuous operation at 0.5 V in PEFC formed using CHbMg3s400900. Cell temperature: 80 °C. Gas humidification temperature: 80 °C. Hydrogen and air were supplied under atmospheric pressure at 50 and 250 cm^3 min^{-1}, respectively.

The current decrease was nearly equivalent to that observed for the PEFC formed using CHb200900 in the previous study (see Figure S2 in the Supporting Information).[13] We showed that the durability increased with an increase in the structure regularity around the Fe−N_4 moiety, which was observed as the peak development at 2.7 Å in the RDF obtained by the EXAFS of CHb200900. However, there was a small peak around 2.7 Å in the RDFs for CHbMg3s400900. Although the detailed reason for the similar durability between CHb200900 and CHbMg3s400900 is not clear at present, it might be associated with the ordered structure of the Fe−N_4 active site in CHbMg3s400900. It is proposed that H_2O_2 generated in the PEFC attacks and decomposes the active site.[33,34] The ordered structure of the Fe−N_4 moiety could be advantageous in avoiding the H_2O_2 attack due to the absence of disordered N, which might be easily attacked. The relatively high durability was also observed for the carbonaceous PEFC cathode catalyst formed using the MgO template, suggesting the possibility that MgO might affect the durability.[9] Further studies are underway to form catalysts with a high durability using the MgO template method and various starting materials for clarifying the effect of MgO.

CONCLUSIONS

Carbonized hemoglobin with substantially developed pores was formed using MgO as the template generated concurrently during the heat treatment from magnesium acetate mixed with hemoglobin to be a starting material mixture. The heme-derived Fe in the carbonized hemoglobin was contained as the Fe−N_4 moiety with limited disorder compared to the heme. The activity for O_2 reduction of the carbonized hemoglobin was dependent on the extent of the pore development. The highly developed pores led to an improvement in the activity and the performance of the PEFC formed using the carbonized hemoglobin in the cathode. The PEFC durability was equivalent to that of the PEFC formed using the carbonized hemoglobin formed through a CO_2 activation process for the pore development. The results indicated that the MgO template method effectively produced pore development in the carbon materials derived from hemoglobin that consequently provided an activity enhancement. The information obtained in this study on the relationships between the activity, the durability, and the catalyst structures would be useful for further enhancement of the catalysis.

ASSOCIATED CONTENT

Supporting Information

Comparison of the fuel cell test results between the present and previous studies (ref 13). This material is available free of charge via the Internet at http://pubs.acs.org.

AUTHOR INFORMATION

Corresponding Author

*E-mail: maruyama@omtri.or.jp. Tel.: +81-6-6963-8043. Fax: +81-6-6963-8049.

ACKNOWLEDGMENTS

The XAFS measurements were performed with the approval of the SPring-8 (Proposals 2008A1891, 2011A1019). This study was partly supported by a Grant-in-Aid for Scientific Research (Project 20560628) given to Y.M. from the Ministry of Education, Culture, Sports, Science and Technology, Japan, for which the authors are grateful.

REFERENCES

(1) Kyotani, T.; Sonobe, N.; Tomita, A. *Nature* **1988**, *331*, 331.
(2) Kyotani, T.; Tsai, L.; Tomita, A. *Chem. Mater.* **1995**, *7*, 1427.
(3) Ma, Z.-X.; Kyotani, T.; Tomita, A. *Chem. Commun.* **2000**, 2365.
(4) Joo, S. H.; Choi, S. J.; Oh, I.; Kwak, J.; Liu, Z.; Terasaki, O.; Ryoo, R. *Nature* **2001**, *412*, 169.
(5) Garsuch, A.; d'Eon, R.; Dahn, T.; Klepel, O.; Garsuch, R. R.; Dahn, J. R. *J. Electrochem. Soc.* **2008**, *155*, B236.
(6) Han, S.; Sohn, K.; Hyeon, T. *Chem. Mater.* **2000**, *12*, 3337.
(7) Ziegelbauer, J. M.; Olson, T. S.; Pylypenko, S.; Alamgir, F.; Jaye, C.; Atanassov, P.; Mukerjee, S. *J. Phys. Chem. C* **2008**, *112*, 8839.
(8) Morishita, T.; Soneda, Y.; Tsumura, T.; Inagaki, M. *Carbon* **2006**, *44*, 2360.
(9) Maruyama, J.; Fukui, N.; Kawaguchi, M.; Hasegawa, T.; Kawano, H.; Fukuhara, T.; Iwasaki, S. *Carbon* **2010**, *48*, 3271.
(10) Maruyama, J.; Abe, I. *Chem. Mater.* **2005**, *17*, 4660.
(11) Maruyama, J.; Abe, I. *Chem. Mater.* **2006**, *18*, 1303.
(12) Maruyama, J.; Okamura, J.; Miyazaki, K.; Abe, I. *J. Phys. Chem. C* **2007**, *111*, 6597.
(13) Maruyama, J.; Okamura, J.; Miyazaki, K.; Uchimoto, Y.; Abe, I. *J. Phys. Chem. C* **2008**, *112*, 2784.
(14) Jaouen, F.; Herranz, J.; Lefèvre, M.; Dodelet, J.-P.; Kramm, U. I.; Herrmann, I.; Bogdanoff, P.; Maruyama, J.; Nagaoka, T.; Garsuch, A.; Dahn, J. R.; Olson, T.; Pylypenko, S.; Atanassov, P.; Ustinov, E. A. *ACS Appl. Mater. Interfaces* **2009**, *1*, 1623.
(15) Steele, B. C. H.; Heinzel, A. *Nature* **2001**, *414*, 345.
(16) Jacobson, M. Z.; Colella, W. G.; Golden, D. M. *Science* **2005**, *308*, 1901.
(17) Bouwkamp-Wijnoltz, A. L.; Visscher, W.; van Veen, J. A. R. *Electrochim. Acta* **1998**, *43*, 3141.
(18) Underwood, J. H.; Gullikson, E. M.; Koike, M.; Batson, P. J.; Denham, P. E.; Franck, K. D.; Tackaberry, R. E.; Steele, W. F. *Rev. Sci. Instrum.* **1996**, *67*, 3372.
(19) Muramatsu, Y.; Harada, R.; Motoyama, M.; Gullikson, E. M. *Tanso* **2009**, *236*, 2.
(20) Muramatsu, Y.; Ueda, S.; Gullikson, E. M. *Tanso* **2009**, *236*, 9.
(21) Maruyama, J.; Abe, I. *Electrochim. Acta* **2003**, *48*, 1443.

(22) Gloaguen, F.; Andolfatto, F.; Durand, R.; Ozil, P. *J. Appl. Electrochem.* **1994**, *24*, 863.
(23) Gojković, S. Lj.; Zečević, S. K.; Savinell, R. F. *J. Electrochem. Soc.* **1998**, *145*, 3713.
(24) Chu, D.; Tryk, D.; Gervasio, D.; Yeager, E. B. *J. Electroanal. Chem.* **1989**, *272*, 277.
(25) Razaq, M.; Razaq, A.; Yeager, E.; DesMarteau, D. D.; Singh, S. *J. Electrochem. Soc.* **1989**, *136*, 385.
(26) Widelöv, A.; Larsson, R. *Electrochim. Acta* **1992**, *37*, 187.
(27) Jones, J. M.; Zhu, Q.; Thomas, K. M. *Carbon* **1999**, *37*, 1123.
(28) Herod, A. J.; Gibb, T. C.; Herod, A. A.; Xu, B.; Zhang, S.; Kandiyoti, R. *Fuel* **1996**, *75*, 437.
(29) Bron, M.; Radnik, J.; Fieber-Erdmann, M.; Bogdanoff, P; Fiechter, S. *J. Electroanal. Chem.* **2002**, *535*, 113.
(30) Watanabe, M.; Sei, H.; Stonehart, P. *J. Electroanal. Chem.* **1989**, *261*, 375.
(31) Maruyama, J.; Sumino, K.; Kawaguchi, M.; Abe, I. *Carbon* **2004**, *42*, 3115.
(32) Proietti, E; Jaouen, F; Lefèvre, M; Larouche, N; Tian, J; Herranz, J; Dodelet, J.-P. *Nat. Commun.* **2011**, *2*, 416.
(33) Lefèvre, M.; Dodelet, J.-P. *Electrochim. Acta* **2003**, *48*, 2749.
(34) Schulenburg, H.; Svetoslav, S.; Schünemann, V.; Radnik, J.; Dorbandt, I.; Fiechter, S.; Bogdanoff, P.; Tributsch, H. *J. Phys. Chem. B* **2003**, *107*, 9034.